Acta Crystallographica Section B
Structural Science
ISSN 0108-7681

Effect of pressure on crystalline L- and DL-serine: revisited by a combined single-crystal X-ray diffraction at a laboratory source and polarized Raman spectroscopy study

Boris A. Zakharov,[a,b]* Boris A. Kolesov[b,c] and Elena V. Boldyreva[a,b]*

[a]Institute of Solid State Chemistry and Mechanochemistry SB RAS, Novosibirsk, Russian Federation, [b]REC-008 Novosibirsk State University, Novosibirsk, Russian Federation, and [c]Institute of Inorganic Chemistry SB RAS, Novosibirsk, Russian Federation

Correspondence e-mail: b.zakharov@yahoo.com, eboldyreva@yahoo.com

Received 26 December 2011
Accepted 12 April 2012

Information on the effect of pressure on hydrogen bonds, which could be derived from single-crystal X-ray diffraction at a laboratory source and polarized Raman spectroscopy, has been compared. L-Serine and DL-serine were selected for this case study. The role of hydrogen bonds in pressure-induced phase transitions in the first system and in the structural stability of the second one are discussed. Non-monotonic distortion of selected hydrogen bonds in the pressure range below $\sim$ 1–2 GPa, a change in the compression mechanism at $\sim$ 2–3 GPa, and the evidence of formation of bifurcated N—H$\cdots$O hydrogen bonds in DL-serine at $\sim$ 3–4 GPa are considered.

1. Introduction

The effect of pressure on crystalline amino acids has attracted much attention in the last decade (Boldyreva, 2007, 2008, 2009; Moggach *et al.*, 2008; Freire, 2010). There are two main reasons for this. First, crystals of amino acids can be considered as biomimetics for peptides. Second, these crystals are interesting to understand the polymorphism of molecular solids, and the relative contributions of hydrogen bonds, electrostatic interactions and van der Waals interactions in the formation of a certain crystal structure and its reconstruction on variation of temperature or pressure. Pressure-induced phase transitions have been reported for several crystalline amino acids, such as glycine (Boldyreva *et al.*, 2004; Boldyreva, Ivashevskaya *et al.*, 2005; Dawson *et al.*, 2005; Goryainov *et al.*, 2005, 2006), L-serine (Kolesnik *et al.*, 2005; Moggach *et al.*, 2005; Moggach, Marshall & Parsons, 2006; Boldyreva, Sowa *et al.*, 2006; Drebushchak *et al.*, 2006), L- and DL-cysteine (Moggach, Allan *et al.*, 2006; Minkov, Tumanov *et al.*, 2010; Minkov, Goryainov *et al.*, 2010). At the same time, some of the crystal structures were shown to be very robust to increasing pressure, showing no polymorphic transitions up to the highest pressures reached in experiments, which were sometimes as high as 23 GPa (α-glycine; Murli *et al.*, 2003), and usually $\sim$ 7–10 GPa.

Hydrogen bonds have been shown to play an important role in the structural stability/instability of crystals in general, and of the crystalline amino acids in particular. Pressure is one of the tools to modify crystal structures and to influence the hydrogen bonds (Holzapfel, 1972; Katrusiak, 1991, 1996, 2003, 2004*a*, 2010; Sikka, 1997; Boldyreva, 2004*a*,*b*). High-precision structural data related to the characteristics of hydrogen bonds can be obtained from variable-temperature diffraction experiments, which make it possible to follow even subtle changes in the electron charge density distribution, proton shifts, distortion of intermolecular and intramolecular bonds. At the same time, for high-pressure diffraction studies *in situ*,

the diffraction data completeness is unavoidably limited and the data are distorted and require tedious (often manual) processing with numerous corrections. Owing to these limitations, very often the structures of organic molecular crystals studied at high pressures are refined assuming fixed intramolecular geometry and even an isotropic approximation for non-H atoms. As a result, many fine effects become simply inaccessible from experiment and escape the attention of a researcher. At the same time there are examples of very precise and detailed experimental diffraction studies of organic and coordination crystalline compounds, in which the changes not only in the intermolecular distances but even in the intramolecular bonds could be followed reliably as a function of pressure. As examples, one can refer to selected old (Boldyreva *et al.*, 1998; Katrusiak, 1990, 1995) and recent publications (Budzianowski & Katrusiak, 2004; Budzianowski *et al.*, 2006; Casati *et al.*, 2009*a*; Dziubek *et al.*, 2010; Fabbiani *et al.*, 2009; Gajda & Katrusiak, 2007; Macchi & Sironi, 2005; Marelli *et al.*, 2011; Olejniczak *et al.*, 2009; Tumanov *et al.*, 2010). The success of these studies was based on applying the special procedures of data collection and reduction (Ahsbahs, 1987, 2004; Angel, 2003; Angel & Finger, 2011; Boldyreva *et al.*, 1999; Casati *et al.*, 2007; Dera & Katrusiak, 1999; Dziubek & Katrusiak, 2002; Girard *et al.*, 2010; Katrusiak, 2001, 2004*b*,*c*, 2008; Kuhs *et al.*, 1996; Naumov & Boldyreva, 1997; Sowa & Ahsbahs, 2006), as well as on various experimental 'tricks' like using multiple crystals to increase the data completeness (Casati *et al.*, 2009*a*,*b*; Johnstone *et al.*, 2010), complementing experimental measurements with model calculations (Johnstone *et al.*, 2008) or using the invariom database (Dittrich *et al.*, 2009).

One more approach to the challenging problem of following the distortions of hydrogen bonds in crystalline amino acids could be based on combining X-ray diffraction studies with Raman spectroscopic experiments. A combination of precise single-crystal X-ray diffraction studies and the polarized Raman spectroscopy of oriented single crystals has proven to be especially informative to follow the changes in hydrogen bonds induced by variations of temperature (Kolesov & Boldyreva, 2007, 2010; Zakharov *et al.*, 2011). To the best of our knowledge, there have not been similar detailed studies of the effect of *pressure* on hydrogen bonds in crystalline amino acids. In fact, the effect of pressure on several amino acids (glycine, L- and DL-alanine, L- and DL-serine, L- and DL-cysteine) has been followed both by X-ray diffraction and Raman spectroscopy (Boldyreva, 2009; Tumanov *et al.*, 2010), but Raman spectra in the above-mentioned studies were measured with non-polarized light, so that the effect of pressure on the individual bonds could not be followed.

The aim of the work described in the present paper was to apply polarized Raman spectroscopy to the oriented single crystals in a diamond–anvil cell (DAC) *in situ*, and to follow the structural changes in essentially the same crystals in the same DAC at the same pressure by single-crystal X-ray diffraction.

We selected single crystals of L- and DL-serine as test compounds as they have already been studied at high pressure *in situ*. Powder samples of L- and DL-serine have been studied by non-polarized Raman spectrocopy (Kolesnik *et al.*, 2005; Murli *et al.*, 2006), X-ray diffraction at a synchrotron source at ESRF (Boldyreva, Sowa *et al.*, 2006) and neutron diffraction (Moggach, Marshall & Parsons, 2006). Single crystals of L-serine have been studied by single-crystal X-ray diffraction using a laboratory source and a four-circle diffractometer at pressures below 4.4 GPa (Boldyreva, Kolesnik *et al.*, 2005) and at 8 GPa (Drebushchak *et al.*, 2006). The cell parameters of DL-serine were followed by single-crystal X-ray diffraction with a point detector at pressures below 8.6 GPa, and the crystal structure was refined at 8.6 GPa (Boldyreva, Kolesnik *et al.*, 2006). Although the bulk compressibility of L- and DL-serine is practically the same up to ~ 5 GPa, when pressure is increased further L-serine undergoes two first-order phase transitions related to the changes in the hydrogen-bond framework, whereas the structure of DL-serine remains stable until the highest pressure achieved in the experiments.

In the present work we wanted to see if a study at multiple pressure points using polarized Raman spectra, oriented single crystals and a laboratory diffractometer with a CCD detector can provide more details on the effect of pressure on the hydrogen bonds in these systems than the previous experiments, and if this additional information can shed more light on the reasons for the different stabilities of L- and DL-serine with respect to structural phase transitions.

2. Experimental

2.1. Samples

DL-Serine was purchased from ICN Biomedicals. The crystals ($0.25 \times 0.15 \times 0.07$ mm, colorless prisms) were obtained by slow evaporation of an aqueous solution saturated at room temperature.

L-Serine was purchased from Aldrich. The crystals ($0.25 \times 0.05 \times 0.05$ mm^3, colorless prisms) were grown as was described in Boldyreva, Kolesnik *et al.* (2005).

2.2. High-pressure generation and measurement

Hydrostatic pressure was generated in a DAC of the 'Almax-Boehler' type with natural diamonds and without beryllium backing plates, which was suitable both for X-ray diffraction and Raman experiments (Boehler, 2006). A steel gasket with an initial thickness of 200 μm was preindented to 100 μm and the hole size was 350 μm. The ruby fluorescence method was used for pressure calibration (Forman *et al.*, 1972; Piermarini *et al.*, 1975), precision ± 0.05 GPa. Propanol-2 was used as the pressure-transmitting medium for DL-serine, a 4:1 methanol–ethanol mixture was used for L-serine, and the crystal was fixed to a culet face of a DAC with vaseline preliminary cooked in methanol. Two different fluids were used for L- and DL- serine for purely technical reasons, but it has been known from previous experiments that neither of these fluids has an effect on the response of L- or DL-serine to pressure. The limit of the hydrostaticity of propanol-2 is lower

Table 1
Experimental details for DL-serine.

For all structures: $C_3H_7NO_3$, M_r = 105.10, monoclinic, $P2_1/n$, Z = 4. Experiments were carried out at 293 K with Mo $K\alpha$ radiation using an Xcalibur, Ruby, Gemini Ultra diffractometer. Refinement was on 66 parameters with 55 restraints. H-atom parameters were constrained.

	0.2 GPa	0.4 GPa	0.6 GPa	0.9 GPa	1.1 GPa	1.3 GPa
Crystal data						
a, b, c (Å)	4.8431 (5), 9.0258 (5), 10.319 (9)	4.8424 (6), 8.9832 (6), 10.250 (11)	4.8307 (12), 8.956 (2), 10.175 (10)	4.8361 (5), 8.9202 (6), 10.123 (8)	4.8329 (5), 8.9119 (6), 10.088 (7)	4.8235 (5), 8.8863 (6), 10.094 (8)
β (°)	100.86 (3)	101.03 (4)	101.33 (5)	101.49 (3)	101.58 (3)	101.69 (3)
V (Å^3)	443.0 (4)	437.6 (5)	431.6 (4)	427.9 (3)	425.6 (3)	423.7 (4)
No. of reflections for cell measurement	2039	1785	906	2084	1788	2027
μ (mm^{-1})	0.14	0.14	0.14	0.15	0.15	0.15
Crystal size	0.25 × 0.15 × 0.07	0.25 × 0.15 × 0.07	0.25 × 0.15 × 0.07	0.25 × 0.15 × 0.07	0.25 × 0.15 × 0.07	0.25 × 0.15 × 0.07
Data collection						
Absorption correction	*GAUSSIAN Absorb* (Angel, 2004)	*GAUSSIAN Absorb* (Angel, 2004)	*GAUSSIAN Absorb* (Angel, 2004)	*GAUSSIAN Absorb* (Angel, 2004)	*GAUSSIAN Absorb* (Angel, 2004)	*GAUSSIAN Absorb* (Angel, 2004)
T_{min}, T_{max}	0.397, 0.474	0.399, 0.473	0.400, 0.473	0.393, 0.472	0.396, 0.473	0.395, 0.472
No. of measured, independent and observed [$I > 2\sigma(I)$] reflections	3890, 368, 295	3587, 372, 313	1715, 438, 277	3825, 442, 364	3353, 438, 349	3981, 435, 369
R_{int}	0.051	0.050	0.078	0.057	0.052	0.047
(sin $\theta/\lambda)_{max}$ (Å^{-1})	0.727	0.726	0.717	0.727	0.726	0.730
Range of h, k, l	$h = -7 \rightarrow 7$, $k = -13 \rightarrow 13$, $l = -5 \rightarrow 5$	$h = -7 \rightarrow 7$, $k = -13 \rightarrow 13$, $l = -5 \rightarrow 5$	$h = -6 \rightarrow 6$, $k = -11 \rightarrow 12$, $l = -7 \rightarrow 8$	$h = -6 \rightarrow 7$, $k = -12 \rightarrow 12$, $l = -5 \rightarrow 5$	$h = -7 \rightarrow 6$, $k = -12 \rightarrow 12$, $l = -5 \rightarrow 5$	$h = -7 \rightarrow 6$, $k = -12 \rightarrow 12$, $l = -5 \rightarrow 5$
Refinement						
$R[F^2 > 2\sigma(F^2)]$, $wR(F^2)$, S	0.028, 0.067, 1.02	0.031, 0.074, 1.07	0.029, 0.047, 0.89	0.031, 0.070, 1.02	0.030, 0.067, 1.04	0.030, 0.068, 1.08
No. of reflections	368	372	438	442	438	435
$\Delta\rho_{max}$, $\Delta\rho_{min}$ (e Å^{-3})	0.11, −0.08	0.12, −0.11	0.13, −0.09	0.12, −0.12	0.11, −0.11	0.11, −0.10

	1.9 GPa	2.5 GPa	3.1 GPa	3.7 GPa	4.4 GPa
Crystal data					
a, b, c (Å)	4.8098 (4), 8.8377 (5), 9.971 (8)	4.7926 (5), 8.7932 (5), 9.907 (9)	4.7708 (6), 8.7429 (7), 9.864 (11)	4.7576 (6), 8.7046 (6), 9.785 (11)	4.7505 (6), 8.6644 (6), 9.725 (11)
β (°)	101.94 (3)	102.14 (4)	102.14 (4)	102.25 (4)	102.35 (4)
V (Å^3)	414.7 (3)	408.1 (4)	402.2 (5)	396.0 (5)	391.0 (4)
No. of reflections for cell measurement	1666	1979	1919	1547	1837
μ (mm^{-1})	0.15	0.15	0.16	0.16	0.16
Crystal size	0.25 × 0.15 × 0.07	0.25 × 0.15 × 0.07	0.25 × 0.15 × 0.07	0.25 × 0.15 × 0.07	0.25 × 0.15 × 0.05
Data collection					
Absorption correction	*GAUSSIAN Absorb* (Angel, 2004)	*GAUSSIAN Absorb* (Angel, 2004)	*GAUSSIAN Absorb* (Angel, 2004)	*GAUSSIAN Absorb* (Angel, 2004)	*GAUSSIAN Absorb* (Angel, 2004)
T_{min}, T_{max}	0.394, 0.473	0.394, 0.474	0.393, 0.474	0.396, 0.474	0.397, 0.474
No. of measured, independent and observed [$I > 2\sigma(I)$] reflections	3261, 413, 350	3895, 389, 329	3631, 360, 312	3026, 358, 307	3625, 354, 301
R_{int}	0.050	0.049	0.048	0.051	0.050
(sin $\theta/\lambda)_{max}$ (Å^{-1})	0.719	0.718	0.721	0.724	0.725
Range of h, k, l	$h = -6 \rightarrow 6$, $k = -12 \rightarrow 12$, $l = -5 \rightarrow 5$	$h = -6 \rightarrow 6$, $k = -12 \rightarrow 12$, $l = -5 \rightarrow 5$	$h = -6 \rightarrow 6$, $k = -12 \rightarrow 12$, $l = -4 \rightarrow 4$	$h = -6 \rightarrow 6$, $k = -12 \rightarrow 12$, $l = -4 \rightarrow 4$	$h = -6 \rightarrow 6$, $k = -12 \rightarrow 12$, $l = -4 \rightarrow 4$
Refinement					
$R[F^2 > 2\sigma(F^2)]$, $wR(F^2)$, S	0.035, 0.080, 1.08	0.031, 0.073, 1.09	0.029, 0.073, 1.03	0.032, 0.080, 1.12	0.032, 0.078, 1.07
No. of reflections	413	389	360	358	354
$\Delta\rho_{max}$, $\Delta\rho_{min}$ (e Å^{-3})	0.14, −0.10	0.13, −0.11	0.13, −0.11	0.11, −0.12	0.11, −0.11

(4.2 GPa) than that of a methanol–ethanol mix (9.8 GPa; Angel *et al.*, 2007), but we were primarily interested in the lower pressure range and did not aim to increase the pressure above 4.5–5 GPa.

Table 2
Experimental details for L-serine.

For all structures: $C_3H_7NO_3$, M_r = 105.10, orthorhombic, $P2_12_12_1$, Z = 4. Experiments were carried out at 293 K with Mo $K\alpha$ radiation using an Xcalibur, Ruby, Gemini Ultra diffractometer. Refinement was on 66 parameters (61 for 5.0 GPa) with 0 restraints. H-atom parameters were constrained.

	0.1 GPa	0.3 GPa	0.5 GPa	0.8 GPa	1.0 GPa
Crystal data					
a, b, c (Å)	5.590 (2), 8.569 (13), 9.233 (7)	5.603 (3), 8.577 (15), 9.231 (8)	5.5885 (14), 8.542 (9), 9.146 (4)	5.5741 (17), 8.436 (9), 9.088 (5)	5.5668 (17), 8.463 (10), 9.072 (5)
V (Å^3)	442.2 (8)	443.7 (9)	436.6 (5)	427.3 (5)	427.4 (6)
No. of reflections for cell measurement	742	737	742	713	713
μ (mm^{-1})	0.14	0.14	0.14	0.15	0.15
Crystal size (mm)	0.25 × 0.05 × 0.05	0.25 × 0.05 × 0.05	0.25 × 0.05 × 0.05	0.25 × 0.05 × 0.05	0.25 × 0.05 × 0.05
Data collection					
Absorption correction	*GAUSSIAN Absorb* (Angel, 2004)	*GAUSSIAN Absorb* (Angel, 2004)	*GAUSSIAN Absorb* (Angel, 2004)	*GAUSSIAN Absorb* (Angel, 2004)	*GAUSSIAN Absorb* (Angel, 2004)
T_{min}, T_{max}	0.388, 0.474	0.387, 0.474	0.389, 0.474	0.388, 0.474	0.395, 0.474
No. of measured, independent and observed [$I > 2\sigma(I)$] reflections	2565, 661, 334	2553, 657, 338	2478, 649, 306	2495, 638, 327	2426, 626, 343
R_{int}	0.094	0.084	0.090	0.084	0.079
(sin $\theta/\lambda)_{max}$ (Å^{-1})	0.749	0.737	0.745	0.740	0.740
Range of h, k, l	$h = -8 \rightarrow 8$, $k = -8 \rightarrow 7$, $l = -12 \rightarrow 12$	$h = -8 \rightarrow 8$, $k = -8 \rightarrow 8$, $l = -12 \rightarrow 12$	$h = -8 \rightarrow 8$, $k = -7 \rightarrow 7$, $l = -12 \rightarrow 12$	$h = -8 \rightarrow 8$, $k = -7 \rightarrow 8$, $l = -11 \rightarrow 11$	$h = -8 \rightarrow 8$, $k = -8 \rightarrow 7$, $l = -12 \rightarrow 11$
Refinement					
$R[F^2 > 2\sigma(F^2)]$, $wR(F^2)$, S	0.064, 0.128, 0.98	0.062, 0.125, 1.01	0.061, 0.152, 0.97	0.065, 0.154, 1.01	0.059, 0.138, 0.98
No. of reflections	661	657	649	638	626
$\Delta\rho_{max}$, $\Delta\rho_{min}$ (e Å^{-3})	0.17, −0.16	0.15, −0.17	0.18, −0.21	0.19, −0.22	0.18, −0.16

	2.1 GPa	3.1 GPa	4.0 GPa	5.0 GPa, phase (II)
Crystal data				
a, b, c (Å)	5.514 (2), 8.396 (11), 8.868 (6)	5.5267 (18), 8.366 (10), 8.812 (5)	5.489 (2), 8.339 (10), 8.632 (6)	5.631 (3), 6.921 (15), 9.619 (8)
V (Å^3)	410.6 (6)	407.5 (6)	395.1 (6)	374.9 (9)
No. of reflections for cell measurement	672	657	557	577
μ (mm^{-1})	0.15	0.15	0.16	0.17
Crystal size (mm)	0.25 × 0.05 × 0.05	0.25 × 0.05 × 0.05	0.25 × 0.05 × 0.05	0.25 × 0.05 × 0.05
Data collection				
Absorption correction	*GAUSSIAN Absorb* (Angel, 2004)	*GAUSSIAN Absorb* (Angel, 2004)	*GAUSSIAN Absorb* (Angel, 2004)	*GAUSSIAN Absorb* (Angel, 2004)
$T_{min,\ T_{max}}$	0.386, 0.474	0.393, 0.474	0.394, 0.473	0.390, 0.474
No. of measured, independent and observed [I > 2$\sigma(I)$] reflections	2298, 582, 310	2257, 588, 298	2131, 549, 254	1637, 365, 241
R_{int}	0.079	0.092	0.130	0.098
(sin $\theta/\lambda)_{max}$ (Å^{-1})	0.745	0.744	0.743	0.624
Range of h, k, l	$h = -8 \rightarrow 8$, $k = -7 \rightarrow 7$, $l = -11 \rightarrow 11$	$h = -8 \rightarrow 8$, $k = -7 \rightarrow 7$, $l = -11 \rightarrow 11$	$h = -8 \rightarrow 8$, $k = -8 \rightarrow 8$, $l = -10 \rightarrow 11$	$h = -7 \rightarrow 7$, $k = -5 \rightarrow 5$, $l = -11 \rightarrow 11$
Refinement				
$R[F^2 > 2\sigma(F^2)]$, $wR(F^2)$, S	0.053, 0.112, 0.93	0.060, 0.123, 0.93	0.065, 0.152, 0.94	0.060, 0.086, 1.02
No. of reflections	582	588	549	365
$\Delta\rho_{max}$, $\Delta\rho_{min}$ (e Å^{-3})	0.15, −0.16	0.17, −0.18	0.17, −0.16	0.14, −0.14

2.3. Single-crystal X-ray diffraction

Data were collected (pressure range for DL-serine 0.2–4.4 GPa, for L-serine 0.1–5.0 GPa) using an Oxford Diffraction Gemini R Ultra X-ray diffractometer with a CCD area detector and Mo $K\alpha$ radiation. The following software was used: *CrysAlis PRO* (Oxford Diffraction, 2010; data collection, cell refinement and data reduction); *SHELXS*97 (Sheldrick, 2008; structure solution); *SHELXL*97 (Sheldrick, 2008) and *X-STEP*32 (Stoe & Cie, 2000; structure refinement). Absorption of X-rays by diamonds was taken into account using *ABSORB* (Gaussian absorption correction; Angel, 2004). The reflections from the sample which overlapped with diamond and gasket reflections were excluded manually. *Mercury* (Macrae *et al.*, 2006) and *PLATON* (Spek, 2009) were used for structure visualization and analysis. *Tensor*

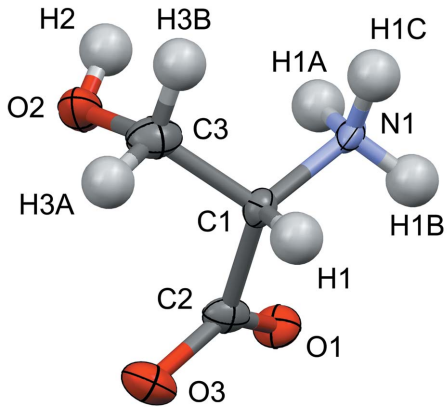

Figure 1
A displacement ellipsoid plot of DL-serine showing the atom-numbering scheme, asymmetric unit and 50% probability displacement ellipsoids at 295 K and 0.9 GPa. H atoms are shown as arbitrary spheres.

(Hazen & Finger, 1982) was used to calculate the anisotropy of lattice strain. CIF files were prepared for publication using *enCIFer* (Allen *et al.*, 2004).

Owing to the fixed orientation of the flat crystal in the DAC, reflections from certain parts of the reciprocal space were under-represented and this resulted in a noticeable distortion of the ellipsoids describing the ADPs for selected atoms and 'chaotic' changes in the ellipsoid shapes *versus* pressure. Since our main focus was on the changes in the distances between non-H atoms in hydrogen bonds, we have analyzed the possible impact of the errors in the anisotropic displacement parameters (ADPs) on the intermolecular distances. The results of refinements in the isotropic approximation for all non-H atoms were compared with those obtained from the anisotropic refinement of non-H atoms with and without restraints (DELU and SIMU with default values for all non-H atoms, and ISOR for C1 atom with effective standard deviation 0.01). Since the shape of the ADP ellipsoids was the best for the anisotropic refinement with restraints, we have used this model in the final CIFs submitted with the manuscript. All H atoms were refined with constraints.[1] Parameters characterizing data collection and refinement, as well as crystal data are summarized in Tables 1 and 2.

2.4. Polarized Raman spectroscopy

Raman experiments were performed in parallel with X-ray diffraction: at each pressure point, after X-ray diffraction data collection three Raman spectra (unpolarized spectrum and two spectra polarized along ***a*** and ***c*** crystallographic directions for DL-serine and along ***a*** and ***b*** + ***c*** directions for L-serine) were recorded; after that the pressure in the DAC was increased and the same sequence of X-ray diffraction and Raman spectra measurements was repeated at the next pressure point. Raman spectra were recorded using a LabRAM HR 800 spectrometer from HORIBA Jobin Yvon with a CCD detector. For spectral excitation the 488 nm line of an Ar^+ laser was used with a beam size of ~ 1 μm on the surface of our sample and ~ 8 mW power. All data were collected using a Raman microscope in backscattering geometry. Spectral resolution was 2 cm^{-1}, but actual broadening of the bands in the spectra was significantly higher due to an increase in anharmonicity with increasing pressure.[2]

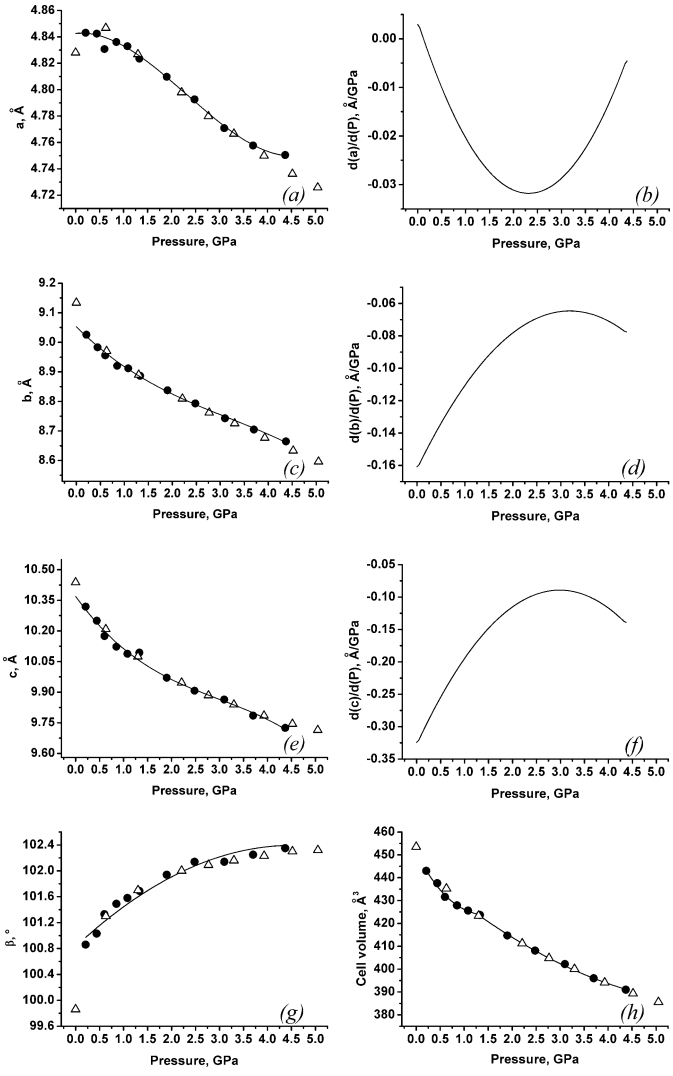

Figure 2
Unit-cell parameters and volume (*a*), (*c*), (*e*), (*g*), (*h*) for DL-serine at different pressures from the present work (black circles) and from Boldyreva, Kolesnik *et al.* (2006) (open triangles), and derivatives of the third-order polynoms which describe the pressure dependencies of the unit-cell parameters (*b*), (*d*), (*f*).

3. Results and discussion

The asymmetric unit and atom-numbering scheme of DL-serine is shown in Fig. 1. Data on the changes in cell para-

[1] Supplementary data for this paper are available from the IUCr electronic archives (Reference: GP5049). Services for accessing these data are described at the back of the journal.

[2] The finite width of a vibrational band is the result of anharmonic coupling of the mode with other modes of low wavenumber by definition, and this manifests itself as the band's broadening at high pressure. Cubic anharmonicity typically is prevalent in solids. An increase in the cubic anharmonicity can be expected due to the shortening of interatomic distances at high pressure.

Table 3
Parameters characterizing linear strain along the principal axes of strain ellipsoid for DL-serine at high pressure (output data of *Tensor*; Hazen & Finger, 1982).

	Angle with		
	$+A$ (Error)	$+B$ (Error)	$+C$ (Error)
Axis 1	11.5 (5)	90 (0)	112.3 (5)
Axis 2	90 (0)	0 (0)	90 (0)
Axis 3	78.5 (5)	90 (0)	22.3 (5)

meters as well as the data on the geometrical parameters of the hydrogen bonds *versus* pressure in L-serine agreed well with those previously reported based on X-ray single-crystal diffraction (Moggach *et al.*, 2005) and powder diffraction (Boldyreva, Sowa *et al.*, 2006; see discussion below). Raman spectra also agreed well with those previously measured (Kolesnik *et al.*, 2005; see supplementary material). As far as we can conclude from the spectra, there is no significant difference in the pressure-induced changes for the same modes in the spectra with different polarizations. This means that there are no significant changes in the relative orientation of molecules in the structure of DL-serine on increasing pressure (which can also be confirmed by single-crystal X-ray diffraction). On the other hand, the rotation of the COO groups with the subsequent formation of bifurcated hydrogen bonds was detected by diffraction and could be confirmed by spectroscopy when the COO symmetric and asymmetric vibrations were studied, as described below. It would not be possible to make such conclusions unambiguously if only one of these two techniques were used.

The problem of a polarized Raman study at high pressure compared with a low-temperature study is that the diamonds are also present in the laser beam while measuring the spectra. This is one of the main reasons why it was not possible to measure the pressure dependence of the ν_s(OH) vibrational frequencies. The wavenumber of the ν_s(OH) mode should be around 3000 cm^{-1} and inevitably strongly overlaps with a group of bands corresponding to CH group vibrations. Besides, on strengthening the hydrogen bond, the corresponding mode can overlap with the mode related to second-order scattering in the diamond spectrum (2050–2600 cm^{-1}). In this case one could investigate intermolecular interactions using the low-wavenumber region of Raman spectra only.

Structural data for DL-serine collected in the DAC at 0.2 GPa agreed well with the previously published data for 'free' crystals (Frey *et al.*, 1973). Structural data at high pressures complemented the results reported earlier: in addition to the cell parameters at pressures from 1 to 4.4 GPa and a structure at 8.6 GPa (Boldyreva, Kolesnik *et al.*, 2006), the changes in cell parameters were measured at multiple points at pressures below 1 GPa (Fig. 2), and the crystal structure was also refined at these pressure points. The values of cell parameters between 1 and 4.4 GPa were, in general, in good agreement with previously published data (Boldyreva, Kolesnik *et al.*, 2006), however, no pronounced maximum in the pressure dependence of cell parameter ***a*** could be observed within experimental error (which is known to be higher for measurements with CCD detectors rather than using point detectors; Herbstein, 2000), but rather a plateau in the very low-pressure range. The pressure dependences of linear strain in the directions of principal axes of strain ellipsoid did not show any striking anomalies (Figs. 3 and 4; Boldyreva, Kolesnik *et al.*, 2006). It has already been observed for some other monoclinic systems that non-monotonic changes in the interatomic distances and even in cell parameters can nevertheless give the monotonic pressure dependence of linear strain and not be related to any structural phase transitions (Boldyreva *et al.*, 1998, 2000). The derivatives of compressibility along axes ***a***, ***b*** and ***c*** changed the sign of the tilt angle tangent in the 2–3 GPa pressure range. This corresponded to a decrease in the compression rate in layers in the ***a*** direction, and an increase in the compression rate in layers in the ***b*** direction, as well as between the layers in the ***c*** direction above these pressures. At lower pressures (below 2–3 GPa) the opposite behavior could be seen.

In addition to the cell parameters, the complete structural data have been refined at multiple pressure points. Changes in the distances between non-H atoms in the hydrogen bonds *versus* pressure were essentially the same for all three approximations used in refinement. A new feature, compared with previously published results, was the non-linear and non-monotonic pressure dependence of the interatomic distances in two types of hydrogen bonds (between amino and carboxylic groups, as well as between amino and hydroxyl groups) in the range 0.4–1.5 GPa; Fig. 5.

The angles between the crystallographic and principal axes of strain ellipsoids are given in Table 3. The direction of the maximum compression of the structure, $P3$, coincided with the direction of the N—H···O hydrogen bonds of one of the types [*i.e.* N1—H1*B*···O2 $(\frac{1}{2}+x, \frac{1}{2}-y, \frac{1}{2}+z)$ and further N1—H1*B*···O3 $(\frac{1}{2}+x, \frac{1}{2}-y, \frac{1}{2}+z)$] and therefore with the direction perpendicular to the layers, Fig. 4. The medium-compressed direction, $P2$, almost coincided with the only O—

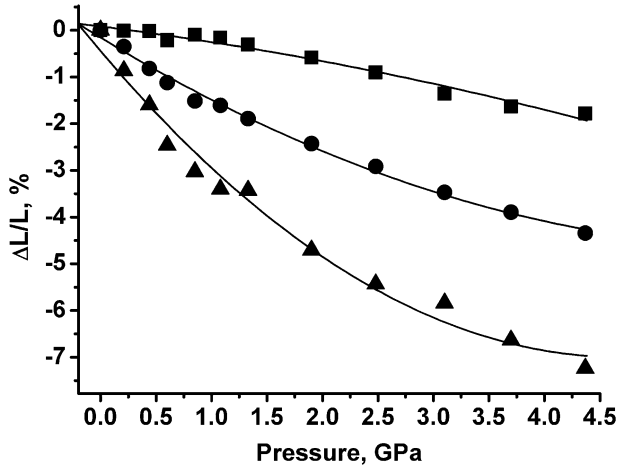

Figure 3
Linear strain in the directions of the principal axes of strain ellipsoids *versus* pressure in DL-serine: squares, circles, triangles define linear strain along axes **1** (minimum compression), **2** (medium compression) and **3** (maximum compression).

H···O-type hydrogen bonds in the structure [O2—H2···O1 ($\frac{1}{2}-x, -\frac{1}{2}+y, \frac{1}{2}-z$)]. The most robust direction in the structure $P1$ corresponded to the compression of the N—H···O hydrogen bonds [N1—H1A···O3 ($\frac{1}{2}-x, -\frac{1}{2}+y, \frac{1}{2}-z$), N1—H1$C$···O3 ($\frac{3}{2}-x, -\frac{1}{2}+y, \frac{1}{2}-z$), Fig. 4].

On increasing pressure from ambient to 4.4 GPa, the carboxylic groups of serine rotated around the C1—C2 bond (see dependencies of torsion angles *versus* pressure in Fig. 6). This rotation resulted in a significant decrease in the N1···O3 distance (Fig. 5) and in the formation of a new hydrogen bond N1—H1B···O3 ($\frac{1}{2}+x, \frac{1}{2}-y, \frac{1}{2}+z$), so that a three-centered (bifurcated) hydrogen bond N1—H1B···(O3, O2) appeared (Fig. 5). An increase in the bifurcated character of the hydrogen bond could also be confirmed by different changes in the symmetric and asymmetric COO vibrations on increasing pressure, since the COO group of DL-serine acts as a proton acceptor in this bifurcated hydrogen bond, and this interaction increases on increasing pressure. In addition, an increase in the intensity of the second N—H···O band on the higher wavenumber side of the intensive CH bands, marked by an arrow in Fig. 7, also confirms the formation of the bifurcated hydrogen bond. An increase in the wavenumbers of the two stretching vibrations of the N—H bonds with pressure, on the right and the left hands from the intensive CH bands, and a change in their relative intensities (see Fig. 7) could result from a change in hydrogen-bond angle due to the rigid rotation of the carboxylic groups. The formation of the bifurcated NH···O hydrogen bonds at high pressure has been observed previously in other crystalline amino acids and was usually related to the structural phase transitions (γ-glycine to δ-glycine; Boldyreva, Ivashevskaya *et al.*, 2004, 2005; β-glycine to β'-glycine; Tumanov *et al.*, 2008; DL-cysteine-II to DL-cysteine-III; Minkov, Tumanov *et al.*, 2010; L-serine-II to L-serine-III; Boldyreva, Sowa *et al.*, 2006). For example, in γ-glycine additional hydrogen bonds strengthen the structure-forming units – head-to-tail chains of zwitterions; this makes the linkages between the chains weaker and facilitates the structural rearrangement in the δ-phase. However, in contrast to the above-mentioned examples, the structure of DL-serine does not undergo a structural phase transition, presumably because the main structural motif (dense hydrogen-bonded double layers with OH···O=C bonds linking the head-to-tail chains of zwitterions within a layer) is very robust. Moreover, the bifurcated hydrogen bond which is formed at high pressure in the DL-serine links the double layers with each other, and this makes the structure even more robust and allows it to avoid a phase transition (Fig. 4).

Rearrangement of the hydrogen-bond network (*i.e.* changes in the bond directions, the formation of the bifurcated hydrogen bonds) was also observed for the crystals of L-serine on increasing pressure and cooling. As has been shown in Moggach *et al.* (2005) and Moggach, Marshall & Parsons (2006), and also confirmed in this paper, for L-serine the bifurcated character of the N—H···O hydrogen bond to the carboxylic group increases at ~ 3–4 GPa, *i.e.* at almost the same pressures as for the DL form (Fig. 8). An increase in the bifurcated character of the hydrogen bond can also be confirmed by changes in the Raman spectra corresponding to COO symmetric and asymmetric vibrations (the same vibration-bond behavior as for DL-serine). The changes in L-serine-I on cooling are related to the positional disorder of O—H···O hydrogen bonds and can also be accompanied by the appearance of bifurcated hydrogen bonds (Kolesov & Boldyreva, 2007). The observed changes for L- and DL-serine are related to the rotation of the COO group around the C1—C2 bond. As a result, the distances to the neighboring H atoms of the hydrogen donors change and new hydrogen bonds are formed. However, in the case of L-serine increasing pressure further leads to a structural phase transition into phase (II) (with a rearrangement of O—H···O hydrogen bonds), in contrast to the racemic crystal. Both in L and DL forms a carboxylic group forms three hydrogen bonds: one of them (A) is formed by one O atom, and the other two (B and C) by the second O atom. The direction of the 'single' hydrogen bond A is almost normal to the plane formed by two other hydrogen bonds B and C from the neighboring oxygen atom

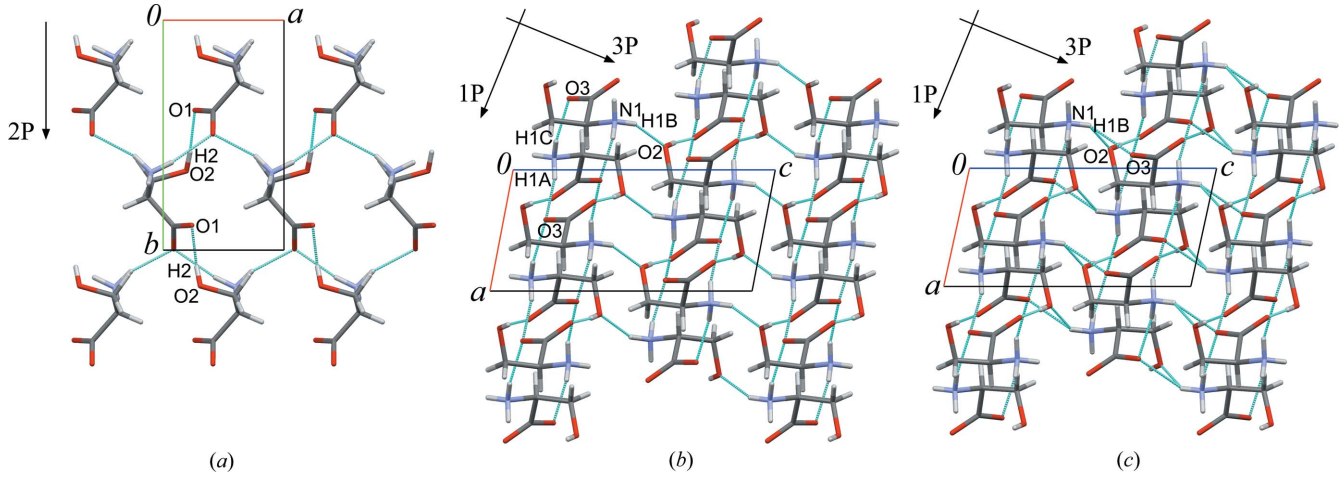

(*a*) (*b*) (*c*)

Figure 4
Fragments of the crystal structure of DL-serine at two pressures: (*a*), (*b*) −0.2 GPa, (*c*) −4.4 GPa. Hydrogen bonds are defined by dashed lines. The directions of the principal axes of strain ellipsoid on cooling and with increasing pressure are shown by arrows. Hydrogen-bond atoms are signed.

(Fig. 8). A change in distances between the molecules (and hence between the neighboring atoms) in the crystal on increasing pressure or on cooling is accompanied by an asymmetric influence on the COO group leading to its rotation out of the plane. The orientation of the carboxylic group is changed because of the influence of the 'single' hydrogen bond; two other bonds are lying in the same plane and so cannot change the COO group orientation (in L-serine) or their influence is balanced (in DL-serine).

Changes in the polarized Raman spectra of DL-serine *versus* pressure were considered in relation to the structural changes revealed by X-ray diffraction. The absence of significant differences between the polarized spectra corresponding to different polarizations confirmed that the mutual orientation of the molecules does not change significantly with pressure. In contrast to low-temperature measurements, for the experiments at high pressures it was not possible to relate the structural changes to the vibrations of selected bonds. No band assignment could be carried out for the low-wavenumber spectral range, whereas the most important vibrations in the high-wavenumber range (like the vibrations corresponding to the O—H···O hydrogen bonds) were shielded by the spec-

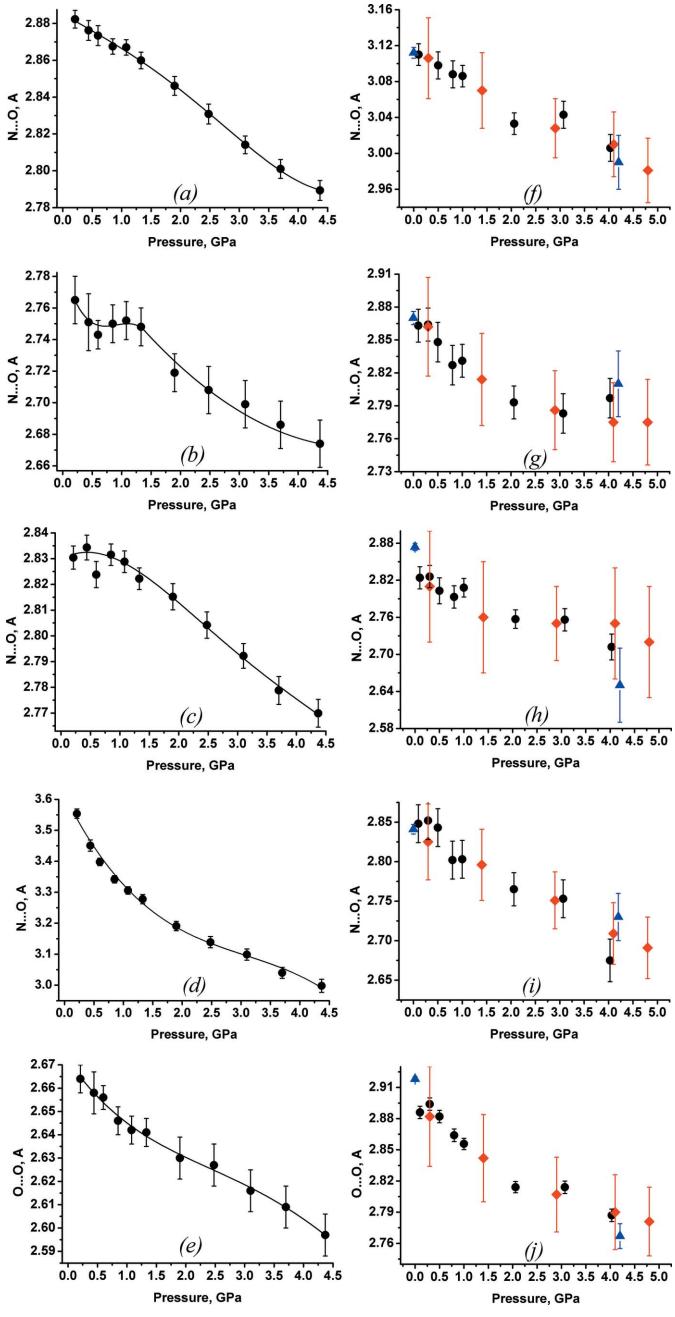

Figure 5
Changes in the interatomic distances of selected hydrogen bonds in DL-serine *versus* pressure: (*a*) N1—H1*A*···O3 $(\frac{1}{2}-x,-\frac{1}{2}+y,\frac{1}{2}-z)$, (*b*) N1—H1*B*···O2 $(\frac{1}{2}+x,\frac{1}{2}-y,\frac{1}{2}+z)$, (*c*) N1—H1C···O3 $(\frac{3}{2}-x,-\frac{1}{2}+y,\frac{1}{2}-z)$, (*d*) N1—H1*B*···O3 $(\frac{1}{2}+x,\frac{1}{2}-y,\frac{1}{2}+z)$, (*e*) O2—H2···O1 $(\frac{1}{2}-x,-\frac{1}{2}+y,\frac{1}{2}-z)$; and in L-serine *versus* pressure: (*f*) N1—H3···O2 $(-1+x,y,z)$, (*g*) N1—H3···O1 $(-1+x,y,z)$, (*h*) N1—H2···O2 $(-\frac{1}{2}+x,\frac{1}{2}-y,2-z)$, (*i*) N1—H1···O1 $(1-x,\frac{1}{2}+y,\frac{3}{2}-z)$, (*j*) O3—H5···O3 $(-\frac{1}{2}+x,\frac{1}{2}-y,1-z)$. The figures contain data from several publications: Present contribution (black circles); Moggach *et al.* (2005) (red rhombs); Boldyreva, Kolesnik *et al.* (2005) at ambient pressure and Boldyreva, Sowa *et al.* (2006) at 4.2 GPa (blue triangles). This figure is in colour in the electronic version of this paper.

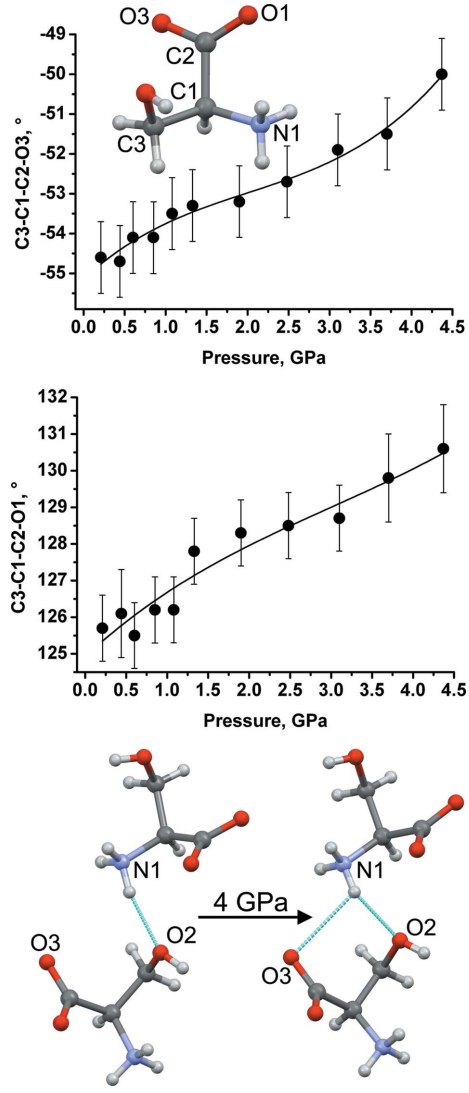

Figure 6
Pressure-induced changes in selected torsion angles in DL-serine with the subsequent formation of bifurcated hydrogen bonds.

trum of diamonds. The vibration bands corresponding to the N—H···O vibrations were very broad, and their shift *versus* pressure could not be measured with reasonable precision.

In a previous contribution by Murli *et al.* (2006), non-motonic (termed 'discontinuous' by the authors of the paper) changes in some of the NH_3 and COO modes in the Raman spectra of DL-serine at ~ 1.5 GPa were also observed. They were interpreted as resulting from some kind of molecular rearrangement in this compound, as well as from a change in the nature of hydrogen-bonding interactions across this pressure. The slopes of several Raman modes changed simultaneously, and this implied a change in the distance dependence of the intermolecular interactions. For example, according to Murli *et al.* (2006), the frequency of the COO wagging mode (750 cm^{-1}) decreased up to 1.5 GPa and started increasing above this pressure, whereas the NH_3 torsional mode also showed a marginal softening up to this pressure and started stiffening above this pressure. In our spectra we did not observe a decrease in the wavenumber of the COO wagging mode below 5 GPa; on the contrary, it increased monotonically in all the pressure ranges studied. Neither could we confirm the 'marginal softening' of the NH_3 mode. However, in the present contribution we have also observed a change in the compression mechanism and the formation of the bifurcated N—H···O hydrogen bond in the 1–3 GPa pressure range, both by diffraction data and by Raman spectra (shown as changes in the COO symmetric and asymmetric vibrations, changes in the intensities and the frequencies of NH stretching modes, and a decrease in the corresponding distance between donor and acceptor atoms). This agrees in general with the observations by Murli *et al.* (2006) and complements them.

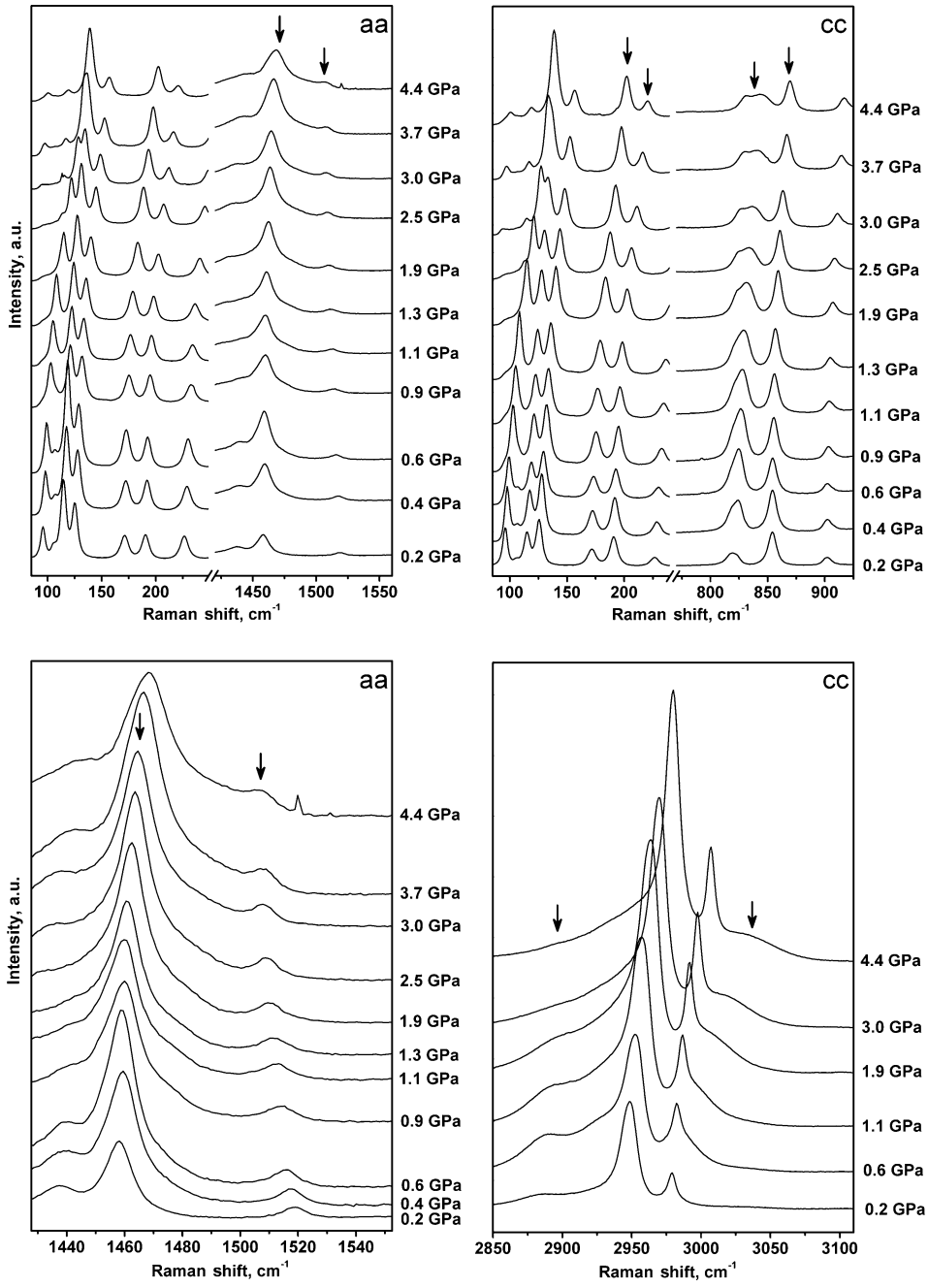

Figure 7
Polarized Raman spectra of DL-serine at high pressures. Symbols **aa** and **cc** define the directions of the polarization vector of the incident (first symbol) and the scattered (last symbol) light with respect to crystallographic axes.

Interesting features in the Raman spectra of DL-serine can be found in the low-wavenumber region, which corresponds to the intermolecular vibrations (the fragments of Raman spectra are shown in Fig. 7). In particular, a redistribution of the intensities of the two libration bands at 171 and 190 cm^{-1} (wavenumbers at 0.2 GPa), and also the merging of low-wavenumber bands in the range between 85 and 135 cm^{-1} can be seen that also confirm the changes in intermolecular interactions and molecular geometry, as shown by single-crystal X-ray diffraction. Raman spectroscopy data have independently confirmed the formation of a bifurcated bond above ~ 3 GPa. A new band at 3030 cm^{-1} appeared at $\sim$ 3–4 GPa, which corresponded to ν_s(NH) stretching vibrations, and the intensity of this band increased

with increasing pressure. An additional confirmation of the formation of the bifurcated hydrogen bond was provided by a decrease in the wavenumber of the asymmetric COO stretching vibrations from 1518 to 1507 cm^{-1} as pressure increased from 0.2 up to 4.4 GPa, and a simultaneous increase in the wavenumber of the symmetric mode from 1457 to 1468 cm^{-1} (Figs. 7 and 9). Thus we can conclude that one of the O atoms of the carboxylic group forms an additional hydrogen bond with an amino group, which agrees with the diffraction data.

Summing up, this study has revealed several new facts which add to our knowledge on the factors determining the stability of a crystal structure with respect to phase transitions on increasing pressure. Thus, although L-serine undergoes two phase transitions at pressures above 5.0 GPa, all the changes in the cell parameters and in the interatomic distances in the hydrogen bonds are monotonic before this pressure is reached. In contrast to that, non-linear and non-monotonic changes in the interatomic distances in some hydrogen-bond lengths and the formation of a bifurcated N—H···O bond were observed in DL-serine, but no structural phase transitions occurred at least below 8.6 GPa. The reason can be sought in a high robustness of the double hydrogen-bonded centrosymmetric layers in the structure of DL-serine, similar to the high stability of the α-polymorph of glycine (Murli *et al.*, 2003).

The structure of L-serine is a three-dimensional framework connected *via* hydrogen bonds. Although this structure is denser than that of DL-serine, there is more space locally around the side $-CH_2OH$ chains. The head-to-tail zwitterion chains act as efficient 'springs' enabling the structure to compress to a certain limit, after which the 'spring' expands backwards and the side $-CH_2OH$ groups rotate cooperatively to change the type of intermolecular O—H···O hydrogen bonding from hydroxyl–hydroxyl to hydroxyl–carboxyl during the first phase transition, or to produce a bifurcated bond during the second one. No change in the compression mechanism occurs within the range of stability of an L-serine phase. In DL-serine, the side chains form hydroxyl–carboxyl hydrogen bonds already at ambient pressure. The 'free space' is distributed in the structure of DL-serine less evenly than in L-serine; dense double layers formed by hydrogen-bonded zwitterions being linked together by longer and, presumably, looser hydrogen bonds. Although this structure resists any radical rearrangements which could be qualified as a phase transition, the co-existence of several types of hydrogen bonds accounts for a change in the compression mechanism with increasing pressure. Below 2–3 GPa, the anisotropy of strain is mainly related to the distortions of the hydrogen bonds within double layers, whereas at higher pressures the contribution to strain which came from the compression of the longer hydrogen bonds between the double layers becomes more significant.

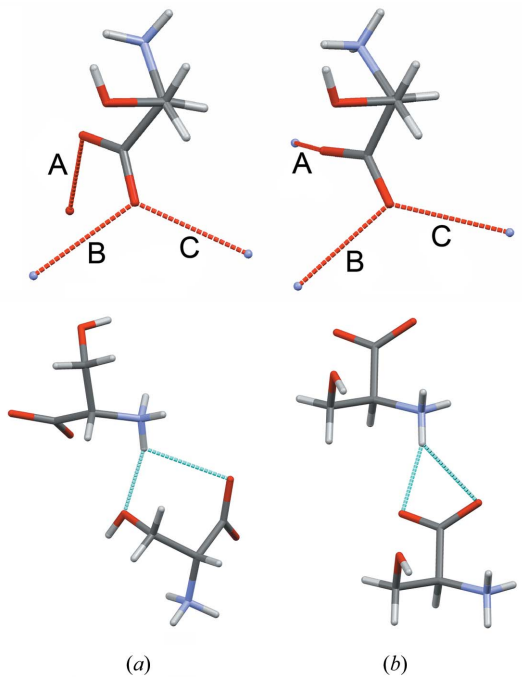

Figure 8
Three hydrogen bonds formed by carboxylic groups in (*a*) DL- and (*b*) L-serine, and bifurcated N—H···O bonds formed on increasing pressure.

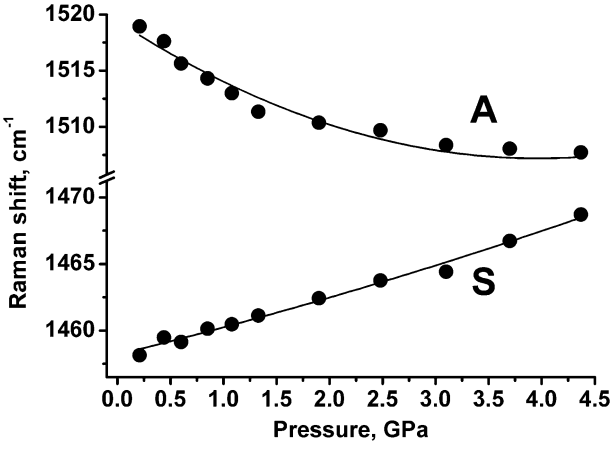

Figure 9
Raman shifts of stretching (symmetric, S, and antisymmetric, A) vibrations of the COO group with increasing pressure.

4. Conclusions

The benefits of combining single-crystal X-ray diffraction and Raman spectroscopy at multiple pressure points for detecting intermolecular interactions and structural distortions manifested themselves in the reliable detection of the formation of a new three-centered N—H···O hydrogen bond in DL-serine at high pressures. A change in the compression mechanism (not related to a phase transition) at *ca* 2 GPa was observed. Some interesting features of these phenomena were partially overlooked in the previous studies.

This work was supported by grants from BRHE (RUX0-008-NO-06) and RFBR (09-03-00451), by the Integration Projects Nos. 13 and 109 of the Siberian Branch of RAS (2009-

2011), and by grant No 16.740.11.0166 from the Russian Ministry of Science and Education. We acknowledge the valuable advice of Dr Francesca Fabbiani on processing the data.

References

Ahsbahs, H. (1987). *Prog. Cryst. Growth Charact. Mater.* **14**, 263–302.
Ahsbahs, H. (2004). *Z. Kristallogr.* **219**, 305–308.
Allen, F. H., Johnson, O., Shields, G. P., Smith, B. R. & Towler, M. (2004). *J. Appl. Cryst.* **37**, 335–338.
Angel, R. J. (2003). *J. Appl. Cryst.* **36**, 295–300.
Angel, R. J. (2004). *J. Appl. Cryst.* **37**, 486–492.
Angel, R. J., Bujak, M., Zhao, J., Gatta, G. D. & Jacobsen, S. D. (2007). *J. Appl. Cryst.* **40**, 26–32.
Angel, R. J. & Finger, L. W. (2011). *J. Appl. Cryst.* **44**, 247–251.
Boehler, R. (2006). *Rev. Sci. Instrum.* p. 77, art. No. 115103.
Boldyreva, E. V. (2004*a*). *Cryst. Eng.* **6**, 235–254.
Boldyreva, E. V. (2004*b*). *J. Mol. Struct.* **700**, 151–155.
Boldyreva, E. V. (2007). *Models, Mysteries, and Magic of Molecules*, edited by J. C. A. Boeyens & J. F. Ogilvie, pp. 169–194. Berlin: Springer Verlag.
Boldyreva, E. V. (2008). *Acta Cryst.* A**64**, 218–231.
Boldyreva, E. V. (2009). *Phase Transitions*, **82**, 303–321.
Boldyreva, E. V., Ivashevskaya, S. N., Sowa, H., Ahsbahs, H. & Weber, H.-P. (2004). *Dokl. Akad. Nauk*, **396**, 358–361.
Boldyreva, E. V., Ivashevskaya, S. N., Sowa, H., Ahsbahs, H. & Weber, H.-P. (2005). *Z. Kristallogr.* **220**, 50–57.
Boldyreva, E. V., Kolesnik, E. N., Drebushchak, T. N., Ahsbahs, H., Beukes, J. A. & Weber, H.-P. (2005). *Z. Kristallogr.* **220**, 58–65.
Boldyreva, E. V., Kolesnik, E. N., Drebushchak, T. N., Sowa, H., Ahsbahs, H. & Seryotkin, Y. V. (2006). *Z. Kristallogr.* **221**, 150–161.
Boldyreva, E. V., Naumov, D. Yu. & Ahsbahs, H. (1998). *Acta Cryst.* B**54**, 798–808.
Boldyreva, E. V., Naumov, D. Yu. & Ahsbahs, H. (1999). *Surface*, **2**, 44–47.
Boldyreva, E. V., Shakhtshneider, T. P., Vasilchenko, M. A., Ahsbahs, H. & Uchtmann, H. (2000). *Acta Cryst.* B**56**, 299–309.
Boldyreva, E. V., Sowa, H., Seryotkin, Yu. V., Drebushchak, T. N., Ahsbhas, H., Chernyshev, V. V. & Dmitriev, V. P. (2006). *Chem. Phys. Lett.* **429**, 474–478.
Budzianowski, A. & Katrusiak, A. (2004). *High-Pressure Crystallography*, edited by A. Katrusiak & P. F. McMillan, pp. 101–112. Dordrecht: Kluwer Academic Publishers.
Budzianowski, A., Olejniczak, A. & Katrusiak, A. (2006). *Acta Cryst.* B**62**, 1078–1089.
Casati, N., Macchi, P. & Sironi, A. (2007). *J. Appl. Cryst.* **40**, 628–630.
Casati, N., Macchi, P. & Sironi, A. (2009*a*). *Chem. Eur. J.* **15**, 4446–4457.
Casati, N., Macchi, P. & Sironi, A. (2009*b*). *Chem. Commun.* **19**, 2679–2681.
Dawson, A., Allan, D. R., Belmonte, S. A., Clark, S. J., David, W. I. F., McGregor, P. A., Parsons, S., Pulham, C. R. & Sawyer, L. (2005). *Cryst. Growth Des.* **5**, 1415–1427.
Dera, P. & Katrusiak, A. (1999). *J. Appl. Cryst.* **32**, 510–515.
Dittrich, B., Hübschle, C. B., Holstein, J. J. & Fabbiani, F. P. A. (2009). *J. Appl. Cryst.* **42**, 1110–1121.
Drebushchak, T. N., Sowa, H., Seryotkin, Y. V., Boldyreva, E. V. & Ahsbahs, H. (2006). *Acta Cryst.* E**62**, o4052–o4054.
Dziubek, K. F., Jeczminski, D. & Katrusiak, A. (2010). *J. Phys. Chem. Lett.* **1**, 844–849.
Dziubek, K. & Katrusiak, A. (2002). *Defect Diffusion Forum*, **208–209**, 319–322.
Fabbiani, F. P. A., Dittrich, B., Florence, A. J., Gelbrich, T., Hursthouse, M. B., Kuhs, W. F., Shankland, N. & Sowa, H. (2009). *CrystEngComm*, **11**, 1396–1406.
Forman, R. A., Piermarini, G. J., Barnett, J. D. & Block, S. (1972). *Science*, **176**, 284–285.
Freire, P. T. C. (2010). *High-Pressure Crystallography*, edited by E. Boldyreva & P. Dera, pp. 559–572. Dordrecht: Kluwer Academic Publishers.
Frey, M. N., Lehmann, M. S., Koetzle, T. F. & Hamilton, W. C. (1973). *Acta Cryst.* B**29**, 876–884.
Gajda, R. & Katrusiak, A. (2007). *Acta Cryst.* B**63**, 896–902.
Girard, E., Fourme, R., Ciurko, R., Joly, J., Bouis, F., Legrand, P., Jacobs, J., Dhaussy, A.-C., Ferrer, J.-L., Mezouar, M. & Kahn, R. (2010). *J. Appl. Cryst.* **43**, 762–768.
Goryainov, S. V., Boldyreva, E. V. & Kolesnik, E. N. (2006). *Chem. Phys. Lett.* **419**, 496–500.
Goryainov, S. V., Kolesnik, E. N. & Boldyreva, E. V. (2005). *Phys. B Condens. Matter*, **357**, 340–347.
Hazen, R. & Finger, L. (1982). *Comparative Crystal Chemistry. Temperature, Pressure, Composition and Variation of the Crystal Structure*. New York: Wiley.
Herbstein, F. H. (2000). *Acta Cryst.* B**56**, 547–557.
Holzapfel, W. B. (1972). *J. Chem. Phys.* **56**, 838–844.
Johnstone, R. D. L., Francis, D., Lennie, A. R., Marshall, W. G., Moggach, S. A., Parsons, S., Pidcock, E. & Warren, J. E. (2008). *CrystEngComm*, **10**, 1758–1769.
Johnstone, R. D. L., Lennie, A. R., Parker, S. F., Parsons, S., Pidcock, E., Richardson, P. R., Warren, J. E. & Wood, P. A. (2010). *CrystEngComm*, **12**, 1065–1078.
Katrusiak, A. (1990). *Acta Cryst.* B**46**, 246–256.
Katrusiak, A. (1991). *Cryst. Res. Technol.* **26**, 523–531.
Katrusiak, A. (1995). *Acta Cryst.* B**51**, 873–879.
Katrusiak, A. (1996). *Crystallogr. Rev.* **5**, 133–180.
Katrusiak, A. (2001). *Z. Kristallogr.* **216**, 646–647.
Katrusiak, A. (2003). *Crystallogr. Rev.* **9**, 87–89.
Katrusiak, A. (2004*a*). *High-Pressure Crystallography*, edited by A. Katrusiak & P. F. McMillan, pp. 513–520. Dordrecht: Kluwer.
Katrusiak, A. (2004*b*). *Acta Cryst.* A**60**, 409–417.
Katrusiak, A. (2004*c*). *Z. Kristallogr.* **219**, 461–467.
Katrusiak, A. (2008). *Acta Cryst.* A**64**, 135–148.
Katrusiak, A. (2010). *High-Pressure Crystallography*, edited by E. Boldyreva & P. Dera, pp. 193–202. Dordrecht: Kluwer Academic Publishers.
Kolesnik, E. N., Goryainov, S. V. & Boldyreva, E. V. (2005). *Dokl. Akad. Nauk*, **404**, 169–172.
Kolesov, B. A. & Boldyreva, E. V. (2007). *J. Phys. Chem. B*, **111**, 14387–14397.
Kolesov, B. A. & Boldyreva, E. V. (2010). *J. Raman Spectrosc.* **41**, 670–677.
Kuhs, W. F., Bauer, F. C., Hausmann, R., Ahsbahs, H., Dorwarth, R. & Holzer, K. (1996). *High Press. Res.* **14**, 341–352.
Macchi, P. & Sironi, A. (2005). *Angew. Chem. Int. Ed.* **44**, 7736–7739.
Macrae, C. F., Edgington, P. R., McCabe, P., Pidcock, E., Shields, G. P., Taylor, R., Towler, M. & van de Streek, J. (2006). *J. Appl. Cryst.* **39**, 453–457.
Marelli, E., Casati, N., Gozzo, F., Macchi, P., Simoncic, P. & Sironi, A. (2011). *CrystEngComm*, **13**, 6845–6849.
Minkov, V. S., Goryainov, S. V., Boldyreva, E. V. & Görbitz, C.-H. (2010). *J. Raman Spectrosc.* **41**, 1458–1468.
Minkov, V. S., Tumanov, N. A., Cabrera, R. Q. & Boldyreva, E. V. (2010). *CrystEngComm*, **12**, 2551–2560.
Moggach, S. A., Allan, D. R., Clark, S. J., Gutmann, M. J., Parsons, S., Pulham, C. R. & Sawyer, L. (2006). *Acta Cryst.* B**62**, 296–309.
Moggach, S. A., Allan, D. R., Morrison, C. A., Parsons, S. & Sawyer, L. (2005). *Acta Cryst.* B**61**, 58–68.
Moggach, S. A., Marshall, W. G. & Parsons, S. (2006). *Acta Cryst.* B**62**, 815–825.
Moggach, S. A., Parsons, S. & Wood, P. A. (2008). *Crystallogr. Rev.* **14**, 143–184.
Murli, C., Sharma, S. M., Karmakar, S. & Sikka, S. K. (2003). *Phys. B Condens. Matter*, **339**, 23–30.

Murli, C., Vasanthi, R. & Sharma, S. M. (2006). *Chem. Phys.* **331**, 77–84.
Naumov, D. Yu. & Boldyreva, E. V. (1997). *Proc. Natl. Conf. Appl. X-rays, Synchrotron, Neutrons and Electrons for Materials Research*, Dubna, JINR, p. 608.
Olejniczak, A., Ostrowska, K. & Katrusiak, A. (2009). *J. Phys. Chem. C*, **113**, 15761–15767.
Oxford Diffraction (2010). *CrysAlisPro*. Oxford Diffraction Ltd, Abingdon, England.
Piermarini, G. J., Block, S., Barnett, J. D. & Forman, R. A. (1975). *J. Appl. Phys.* **46**, 2774–2780.
Sheldrick, G. M. (2008). *Acta Cryst.* A**64**, 112–122.
Sikka, S. K. (1997). *Indian J. Pure Appl. Phys.* **35**, 677–681.
Sowa, H. & Ahsbahs, H. (2006). *J. Appl. Cryst.* **39**, 169–175.
Spek, A. L. (2009). *Acta Cryst.* D**65**, 148–155.
Stoe & Cie (2000). *X-STEP*32. Stoe & Cie GmbH, Darmstadt, Germany.
Tumanov, N. A., Boldyreva, E. V. & Ahsbahs, H. (2008). *Powder Diffr.* **23**, 307–316.
Tumanov, N. A., Boldyreva, E. V., Kolesov, B. A., Kurnosov, A. V. & Quesada Cabrera, R. (2010). *Acta Cryst.* B**66**, 458–471.
Zakharov, B. A., Kolesov, B. A. & Boldyreva, E. V. (2011). *PhysChemChemPhys.* **13**, 13106–13116.